ELSEVIER

Contents lists available at ScienceDirect

Journal of Energy Chemistry



journal homepage: www.elsevier.com/locate/jechem

Photocatalytic one-step synthesis of Ag nanoparticles without reducing agent and their catalytic redox performance supported on carbon

Lingling Shui^a, Guoxiu Zhang^a, Bin Hu^b, Xingxing Chen^c, Mingliang Jin^a, Guofu Zhou^{a,d,e}, Nan Li^{d,*}, Martin Muhler^{b,f,*}, Baoxiang Peng^{b,f,*}

- ^a Guangdong Provincial Key Laboratory of Optical Information Materials and Technology & Institute of Electronic Paper Displays, South China Academy of Advanced Optoelectronics, South China Normal University, Guangzhou 510006, Guangdong, China
- ^b Laboratory of Industrial Chemistry, Ruhr-University Bochum, D-44780 Bochum, Germany
- ^c School of Chemical Engineering, University of Science and Technology Liaoning, Anshan 114051, Liaoning, China
- ^d Shenzhen Guohua Optoelectronics Tech. Co. Ltd, Shenzhen 518110, Guangdong, China
- ^e Academy of Shenzhen Guohua Optoelectronics, Shenzhen 518110, Guangdong, China
- ^f Max Planck Institute for Chemical Energy Conversion, D-45470 Mülheim an der Ruhr, Germany

Dedicated to the 70th anniversary of Dalian Institute of Chemical Physics, CAS, China.

ARTICLE INFO

Article history: Received 30 January 2019 Revised 28 March 2019 Accepted 8 April 2019 Available online 13 April 2019

Keywords:
Silver
Carbon
Photoreduction
Hydrogenation
Oxygen reduction reaction

ABSTRACT

Synthesis of silver nanoparticles (Ag NPs) with state-of-the-art chemical or photo-reduction methods generally takes several steps and requires both reducing agents and stabilizers to obtain NPs with narrow size distribution. Herein, we report a novel method to synthesize Ag NPs rapidly in one step, achieving typical particle sizes in the range from 5 to 15 nm. The synthesis steps only involve three chemicals without any reducing agent: AgNO₃ as precursor, polyvinylpyrrolidone (PVP) as stabilizer, and AgCl as photocatalyst. The Ag NPs were supported on carbon and showed excellent performance in thermal catalytic *p*-nitrophenol reduction and nitrobenzene hydrogenation, and as electrocatalyst for the oxygen reduction reaction

© 2019 Science Press and Dalian Institute of Chemical Physics, Chinese Academy of Sciences. Published by Elsevier B.V. and Science Press. All rights reserved.



Nan Li. Our research covers material science, chemistry and optoelectronics. Main focus is on advanced materials synthesis and their electronic application. The materials include polymers, Ag nanoparticles/nan rods, ZnO-supported nanocomposites. Photochemical, chemical, and physical methods have been used or developed during synthesis research. Both optical and electrical properties of the synthesized materials have been heavily studied.



Matin Muhler's Group for Industrial Redox Catalysis. Our group performs fundamental research in the area of heterogeneous redox catalysis and aims to develop catalysts based on mechanistic insight. The examined reduction reactions comprise Fischer-Tropsch synthesis and the synthesis of methanol and higher alcohols. Oxidation catalysis focuses on the oxidative dehydrogenation of hydrocarbons and the selective oxidation of alcohols and hydrocarbons in the gas phase and in the liquid phase. Recently, we entered the fields of electrocatalysis (e.g., HER, OER, ORR and electrooxidation of alcohols) and photocatalysis (e.g., photocatalytic CO₂ reduction or hydrogen generation via water splitting).



Baoxiang Peng's Group for Three-Phase Catalysis. Our research interest is heterogeneous redox catalysis in the liquid phase under mild conditions. Reduction catalysis focuses on the hydrogenation of nitrobenzene and hydrodeoxygenation of biomass-derived platform chemicals such as glycerol and 5-hydroxymethylfurfural, whereas oxidation reaction comprises the selective oxidation of short chain alcohols and the challenging C-H bond activation of hydrocarbons. *In situ* attenuated total reflection infrared spectroscopy is used to investigate reaction mechanisms of liquid-phase redox reactions.

E-mail addresses: nan.li@guohua-oet.com (N. Li), muhler@techem.rub.de (M. Muhler), baoxiang.peng@techem.rub.de (B. Peng).

^{*} Corresponding authors.

1. Introduction

In recent years, noble-metal nanoparticles have received considerable interest because of their enhanced performance across a diverse range of fields. Among them, silver nanoparticles (Ag NPs) are currently the most widely commercialized nanomaterial. Ag NPs are applied in catalysis, energy, optoelectronics, photochemistry, and medicine [1,2]. It is also well known that silver-based compounds are highly toxic to microorganisms [3]. This property makes silver an excellent choice for medical applications. Moreover, silver is a catalyst with a long history in lab and industry, for example, in ethylene epoxidation.

Various Ag NPs synthesis processes have been developed, including chemical synthesis, physical synthesis, photochemical synthesis, and biological synthesis [4-7]. Among all synthesis processes, chemical reduction is the most frequently applied method for the preparation of Ag NPs. Reduction of noble metal salts, including silver nitrate, is one of the most popular approaches [8-10]. Initially, the reduction of Ag⁺ ions leads to the formation of silver atoms, followed by agglomeration into oligomeric clusters. These clusters eventually turn into colloidal Ag NPs. When the nanoparticle size is much smaller than the wavelength of visible light, the colloidal solution shows different colours depending on particle size and shape [11]. The key challenge for large-scale applications is to achieve long-term-stable Ag NPs in a well-controlled process in terms of particle size and surface chemistry. Therefore, stabilizers are commonly used in combination with reducing agents, for example, the reduction of AgNO₃ with NaBH₄ at room temperature [12], or with ethylene glycol in the presence of polyvinylpyrrolidone (PVP), the so-called polyol process [13]. Normally, it yields 10 nm particles with a narrow size distribution. Ag NPs can also be obtained by direct photo-reduction of AgNO₃ in aqueous Triton X-100 [14] or carboxymethylated chitosan (CMCTS) with UV light [15]. Both Triton X-100 and CM-CTS serve simultaneously as reducing agents for the silver cations and stabilizing agents. 2-8 nm Ag NPs can be synthesised by this method. It has been reported by Zhou et al. [16] that Ag nanorods and dendrites can be obtained by photo-reduction of silver nitrate with polyvinylalcohol using UV irradiation. However, the process takes several hours under different temperatures rendering the synthesis complex. To the best of our knowledge, almost all reported photo-reduction processes require both reducing agents

Despite the success of the individual synthetic routes, the challenge of producing truly reproducible and highly homogeneous Ag NPs still remains. The lack of morphological control over the Ag NPs and the residual surfactants and reducing agents have significant impact on the accessibility of the Ag surface. Hence, it limits the function and applicability, especially in catalysis and medicine applications. Single reduction will typically result in a broad range of particle size (30–150 nm) and diverse shapes, e.g., spheres, rods, and plates [17–19]. Several functional agents including solvents, reducing agents and stabilizers are introduced into different stages during the synthesis process to control the morphology and particle size [20,21]. This often induces long and complicated processes. Therefore, it is difficult to reproduce and control such a process, which is one of the key objectives of this work.

Carbon nanotubes (CNTs) have cylinder structure with one or more layers of graphene. All carbon atoms are bound in a hexagonal lattice except at the end in a perfect structure [22]. Multiwalled carbon nanotubes (MWCNTs) have very good mechanical and thermal stability with high conductivity. Therefore, they were first used as electrical conductive fillers in plastics. Its high surface area also renders CNTs a good candidate for catalytic applications [23,24]. Many studies have indicated an enhanced performance by employing CNTs as catalyst support [25,26].

Nanocomposites have been developed with numerous applications in the last decades, which can provide improved performance, higher stability or resistance, and economic benefit. Noble metal NPs, for practical applications, are often supported by carbon-based materials [27–30]. Research on Ag nanocomposites has been well established, e.g., Ag NPs growing on graphene oxide [31] and ZnO [32] by different reduction agents, resulting in enhanced performance [30].

This work aims at developing an efficient and highly reproducible method for the synthesis of Ag NPs supported on carbon materials in a well controllable way without using reducing agents. The developed method combines the advantages of both photochemical and chemical reactions. Ag NPs were synthesized by using $AgNO_3$ aqueous solutions containing PVP as stabilizer and NaCl to form AgCl as photocatalyst with natural indoor daylight as light source. Both the morphology of the composites and their catalytic activities in p-nitrophenol reduction, nitrobenzene hydrogenation, and oxygen reduction reaction were investigated.

2. Experimental

2.1. Materials

Sodium chloride (AR grade, Alfa Aesar), silver nitrate (AR grade, Sigma-Aldrich), PVP (M.W. 10,000, AR grade, Sigma-Aldrich), activated carbon (AC) and CNTs (Baytubes® C 150 P, Bayer AG) were applied in the synthesis. NaBH₄ (AR grade, Fluka) and *p*-nitrophenol (AR grade, Sigma-Aldrich) were used for catalytic characterization. All chemicals and materials except CNTs were used as received without further treatment. Pristine CNTs were first washed with 1.5 M HNO₃ solution at room temperature for 72 h to remove the residual growth catalyst. Purified CNTs were treated in nitric acid vapour at 200 °C under reflux for 48 h to obtain oxygenfunctionalized CNTs (OCNTs) before use. A detailed description of the preparation of OCNTs can be found elsewhere [33]. Deionized water was used in all experiments. All glassware and instruments were rinsed by deionized water before use.

2.2. Synthesis of Ag NPs and Ag/carbon nanocomposites

The typical synthesis protocol of Ag NPs in solution comprises the following steps: $55\,\mathrm{mg}$ PVP (0.5 mmol of PVP monomer) and $340\,\mathrm{mg}$ AgNO $_3$ (2 mmol) were first dissolved in $400\,\mathrm{mL}$ deionized water, and then 2 mL NaCl ($20\,\mathrm{mM}$) aqueous solution was added to the AgNO $_3$ solution. The solution was exposed to natural light with agitation for $10\,\mathrm{min}$. Different amounts of PVP and NaCl were used, and the synthesis was optimized based on the optical properties of the solution.

The typical synthesis procedure of Ag/carbon nanocomposite consists of the following steps: Ag NP-containing solution was synthesized first according to the protocol as mentioned above. Then, the carbon support (2.16 g) was added to the solution under agitation. The composites were labelled as Ag-AC for activated carbon support and Ag-OCNT for OCNT support (Fig. 1a). Alternatively, the carbon support was added to the solution right after introducing NaCl aqueous solution, and then the mixed solution was exposed for 10 min to natural light. These samples were named as AC-Ag for the activated carbon support and OCNT-Ag for the OCNT support (Fig. 1b). After synthesis, all samples were centrifuged and subsequently dried in an oven overnight before further characterization or catalytic tests.

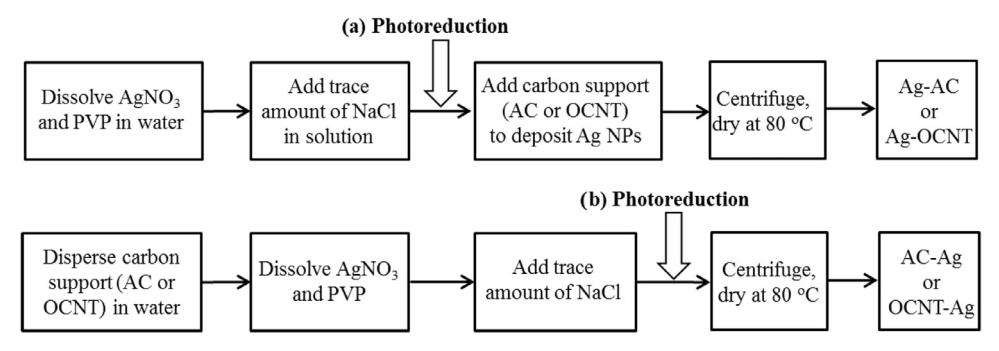


Fig. 1. Different synthesis procedures: (a) sequential Ag NP synthesis-deposition method and (b) simultaneous Ag NP synthesis-deposition method.

2.3. Catalyst characterization

 N_2 physisorption was carried out at $-196~^\circ C$ using a NOVA 2000 series analyzer (Quantachrome Instruments). Prior to each measurement, the sample was first degassed at 200 $^\circ C$ for 2 h. The Ag content was determined by atomic absorption spectroscopy (AAS) (Hitachi Z-2000). X-ray diffraction (XRD) patterns were recorded using a PANalytical Empyrean Bragg-Brentano θ - θ diffractometer with Cu K_α radiation. Transmission electron microscopy (TEM) measurements were carried out with a JEOL JEM-2100HR instrument. The TEM samples were prepared by dispersing the catalyst powder in ethanol under ultrasonication for 30 min and dropping the suspension on a copper grid.

2.4. Catalytic tests

The reduction of p-nitrophenol to p-aminophenol with NaBH₄ was employed to evaluate the catalytic activities of the prepared Ag-based catalyst. The reduction progress was followed with a UV-Vis spectrometer (Lambda 950, PerkinElmer) by monitoring the UV absorption of p-nitrophenol at 400 nm and the absorption of the product p-aminophenol at 300 nm. In a typical measurement, 2 mg carbon supported Ag NPs was added to 3 mL solution containing p-nitrophenol (0.1 mM) and NaBH₄ (0.12 M), and the spectra were repeatedly recorded every 2 min in the range of 200–500 nm until the reaction was finished. The baseline shift had been eliminated when plotting the spectrum.

Nitrobenzene hydrogenation was carried out in a continuous fixed-bed flow reactor in the gas phase (see Fig. S1 in the Supporting Information). The tubular quartz reactor was packed with 0.1 g of catalyst diluted with 1 g of quartz sand. Prior to the reaction, the catalyst was activated with 100 mL/min of 10 vol% H₂ in He at 350 °C for 1 h. The reaction was then performed by feeding a reactant gas mixture containing 0.3 mL/min of nitrobenzene, 9 mL/min of H2 and 90.7 mL/min of He into the reactor at atmospheric pressure and temperatures ranging from 200 to 350 °C with an interval of 25 °C. A constant nitrobenzene flow (0.3 mL/min) was obtained by passing He through two nitrobenzene saturators at 80 °C. The duration of the catalytic test was 1 h for each temperature except at the highest temperature of 350 °C, which was tested for 12 h to evaluate the stability of the catalyst. The effluent products were analyzed every 10 min by an online gas chromatograph (Shimadzu GC-2014) equipped with a Valco sampling loop, a flame ionization detector (FID) and a HP-5 column.

The electrochemical measurements were conducted at room temperature using a CH Instrument (CHI760E, China) in combination with a rotating disk electrode having an area of 0.2472 cm² (PINE Research Instrumentation, USA) in 0.1 M NaOH. Ag/AgCl/3 M KCl and Pt-mesh electrode were used as reference and counter

electrode, respectively. For the preparation of the catalyst ink, 5 mg of the catalyst powder was dispersed in a mixture of water, ethanol and Nafion (5%) using a volume ratio of 490:490:20, respectively, with the aid of ultrasonication for 30 min. A catalyst suspension of 10.4 µL was dropped on the glassy carbon electrode, which corresponds to a loading of 0.210 mg cm⁻². The electrode was left to dry at room temperature in air for at least 30 min before being applied in the oxygen reduction reaction (ORR). The potential was scanned between 0 and -1 V (vs. Ag/AgCl/3 M KCl) at a scan rate of $5 \,\mathrm{mV}$ s⁻¹. The presented electrocatalytic currents were obtained by subtracting the current recorded with the electrolyte saturated with Ar from the currents measured under O₂-saturated conditions. The potentials were reported with respect to the reversible hydrogen electrode (RHE) scale, according to the conversion $E = E_0 + E_{Ag/AgCl} + 0.059 \times pH$ -iRs, where E_0 is the measured potential vs. Ag/AgCl/3 M KCl, $E_{Ag/AgCl}$ is the standard potential of the Ag/AgCl/3 M KCl reference electrode with respect to the standard hydrogen electrode at zero pH, 0.207 V for this case. i is the background-subtracted current measured in the O_2 -saturated solution. Rs is the electrolyte resistance, which was obtained directly from the CHI software at the open circuit potential.

3. Results and discussion

3.1. Ag NPs, Ag/carbon composite preparation and characterization

Under the action of light, silver nitrate decomposes to metallic silver which generally appears black. This process produces large Ag/Ag_2O grains in an uncontrolled way. Because of their light sensitivity, silver halides together with silver nitrate have been extensively used in photographic films and papers. A silver halide particle generates an electron-hole pair when absorbing a photon. Subsequently, the photo-generated electron combines with an Ag^+ ion, which will be reduced to form an Ag^0 atom, whereas the photogenerated holes oxidize H_2O to O_2 [34–37].

By adding trace amounts of NaCl to the AgNO₃ solution, AgCl is formed. In the presence of sunlight, AgCl absorbs photons to generate electrons, which reduce Ag⁺ to Ag⁰. With PVP as stabilizer, Ag NPs are well dispersed in the aqueous solution. Different amounts of NaCl solution were added to the AgNO₃ solution before exposure to sunlight, resulting in different concentrations of Cl⁻ in the solution (1, 0.1, and 0.01 mM).

As can be seen from the pictures in Table S1 (Supporting Information), the solution changed from transparent to pink/light-orange, which is an indication of Ag NP formation. When there was no NaCl present in the solution, the colour did not change even after 30 min, indicating a much lower reaction rate compared with that in the presence of AgCl. A significant colour change was

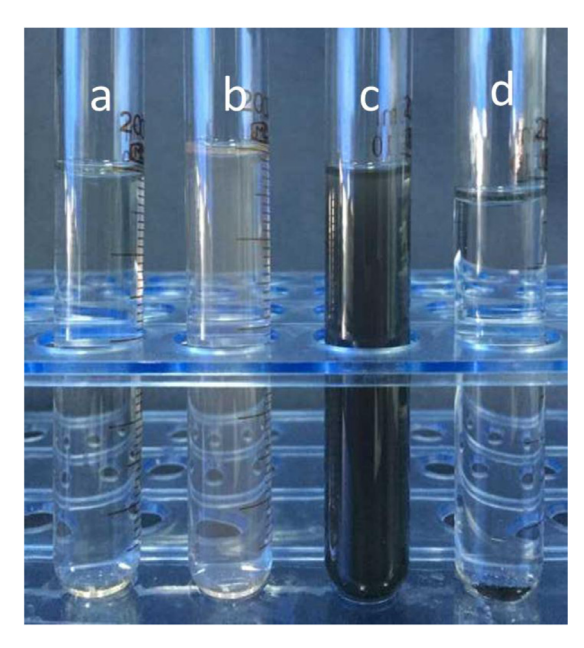


Fig. 2. Synthesis of Ag NPs supported on AC: (a) $AgNO_3-PVP$ solution, (b) after adding NaCl under sunlight, (c) after adding AC to the solution, and (d) after centrifugation to obtain Ag/AC at the bottom.

observed for the 0.01 mM solution after 15 min. The solution started to change in colour after 10 min, when the concentration of Cl $^-$ was 0.1 mM in the AgNO $_3$ solution, and it started to change significantly after 5 min at the Cl $^-$ concentration of 1 mM. This result implies that the amount of Cl $^-$ plays a key role in the Ag NPs reduction rate. More Cl $^-$ can generate more AgCl nuclei, and, accordingly, more electrons resulting in a higher reaction rate of Ag NP formation.

Different amounts of PVP were tested during the Ag NP synthesis. The molar ratio between PVP monomer and AgNO₃ was varied from 1:1 to 1:8. As can be seen from Table S2 (Supporting Information), the solution changed to different colours as a function of the amount of PVP. The colour also appeared at different periods of time during the exposure to sunlight. This result indicates that the amount of PVP has an impact on the shape and size of Ag NPs. As seen from Fig. 2, the original AgNO₃/PVP solution is transparent. After adding NaCl to the solution, it becomes light-orange, indicating the formation of Ag NPs. After adding the carbon support (AC) to the Ag NPs solution followed by centrifugation, the colour of the solution changes from light-orange to transparent due to the deposition of Ag NPs on AC.

In the case of nanoscale metal particles, the absorption wavelength associated with the s-p transitions depends on the shape and size of the particles. This is a unique property of NPs due to the fact that the s-p (conduction) electrons are largely free to move throughout the NP, and their energies are therefore sensitive to the shape and size. For Ag NPs, the colour depends on their morphology and shape. The colour change of the solution from transparent to red/pink is a clear indication of Ag NP formation. When nanoparticles aggregate, the wavelengths of absorbed light change rationalizing the colour difference among the samples prepared from different amount of PVP.

The UV-Vis spectra of Ag NPs were taken after exposure to natural light for different periods of time. As shown in Fig. 3, the characteristic plasmon band of Ag at 380 nm after 7 and 14 min exposure indicates the presence of Ag NPs. However, there was no Ag NPs formation even after 14 min exposure without NaCl, indicating that Cl and light exposure are the key factors in this Ag NPs synthesis strategy.

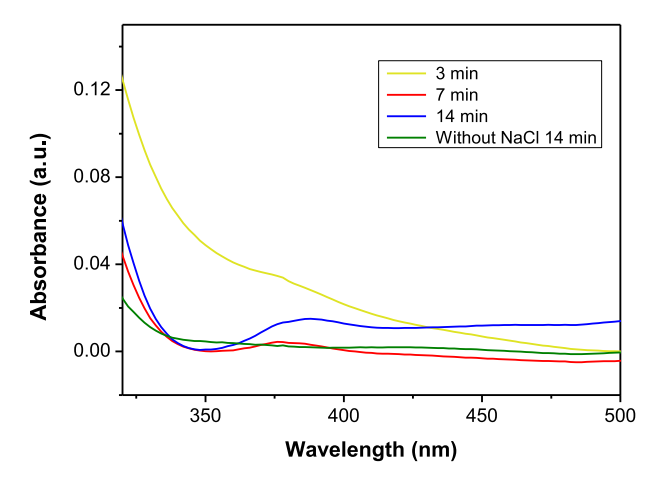


Fig. 3. UV-Vis spectra of Ag NPs after exposure to natural light.

Table 1. BET specific surface areas and Ag loadings determined by AAS.

Samples	AC	OCNT	Ag-AC	AC-Ag	Ag-OCNT	OCNT-Ag
Surface area (m ² g ⁻¹)	650	283	473	507	268	258
Ag loading (wt%)	-	-	2.6	2.7	1.8	1.2

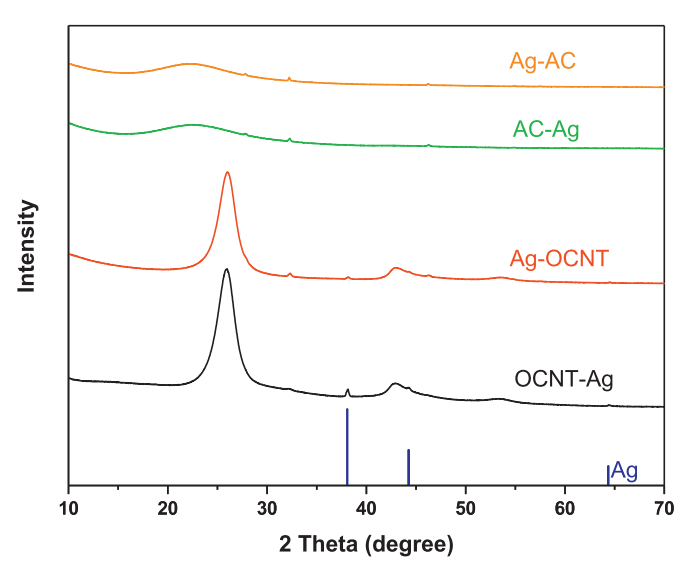


Fig. 4. XRD patterns of synthesised catalysts.

The specific surface areas and Ag loadings of the prepared carbon-supported catalysts are summarized in Table 1. The specific surface areas of AC- and OCNT-supported catalysts were close to those of the parent materials amounting to 650 m² g⁻¹ and 283 m² g⁻¹, respectively. The addition of the carbon support before or after Ag NP formation did not show a significant effect on the specific surface area. Ag loadings for Ag-AC, AC-Ag, Ag-OCNT and OCNT-Ag are 2.6, 2.7, 1.8 and 1.2 wt%, respectively. Compared with OCNT-supported Ag catalysts, AC-supported catalysts have higher Ag loadings, which is probably due to the higher specific surface area.

The XRD patterns of the prepared samples are shown in Fig. 4. AC-supported catalysts only show typical features of

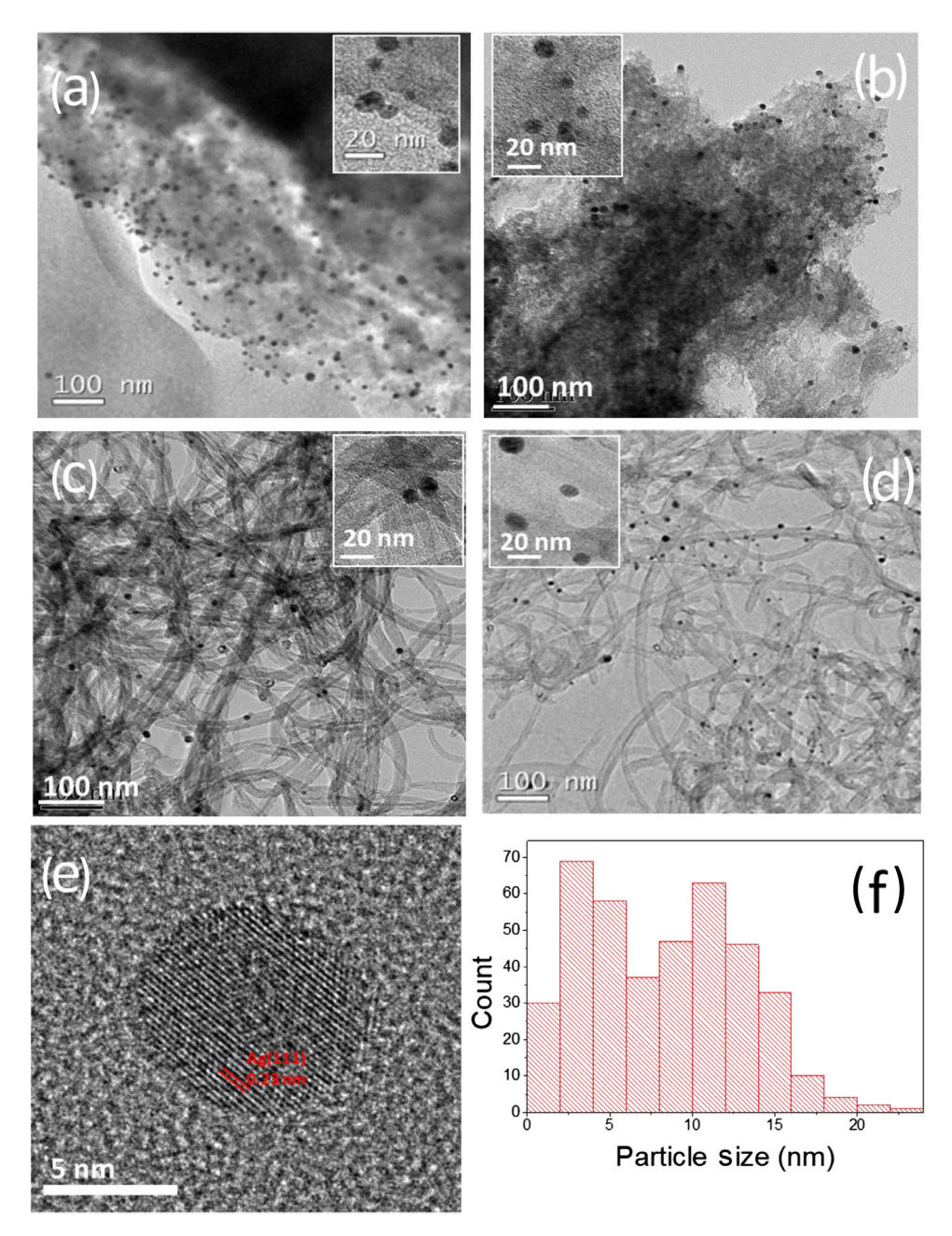


Fig. 5. High resolution TEM images of (a) Ag-AC, (b) AC-Ag, (c) Ag-OCNT, (d) OCNT-Ag; (e) magnified TEM image of Ag NPs in OCNT-Ag, (f) particle size distribution of the synthesised Ag NPs.

amorphous carbon, but no reflections of metallic Ag indicating highly dispersed small Ag particles. In comparison, both Ag-OCNT and OCNT-Ag show very small reflections at 38.1°, 44.2° and 64.4° due to metallic Ag NPs, indicating the successful synthesis of OCNT-supported Ag catalysts and the absence of large Ag particles. Furthermore, the small reflection at 32.3° (PDF# 00-001-1013) suggests a minor content of AgCl for all 4 samples.

In order to assess the Ag NP morphology, high-resolution TEM was used to characterise all 4 samples. As can be seen from Fig. 5, the Ag NPs are well dispersed on all samples. Fig. 5(a and b) is image of samples originating from adding AC to the solution before (Ag-AC) and after Ag NP (AC-Ag) formation, respectively. Fig. 5(c and d) is image of samples obtained by adding OCNTs to the solution before (Ag-OCNT) and after Ag NP (OCNT-Ag) formation, respectively. Furthermore, the lattice fringe spacings of Ag

NPs in OCNT-Ag are determined to be 0.23 and 0.20 nm representing Ag (111) and Ag (200) lattice planes (Fig. 5e and Fig. S2), respectively. Fig. 5(f) shows a representative particle size distribution of the Ag-AC sample in the range up to 15 nm. Other samples show similar particle size distributions, which is consistent with the XRD results. There is no significant difference between adding the carbon support before or after the Ag NP formation.

Homogeneous deposition of Ag NPs with narrow particle size distribution on the carbon supports demonstrates the advantages of the photocatalytic one-step synthesis. Because the trace amount of AgCl is well dispersed in the solution without precipitation, it acts as photocatalyst reducing Ag⁺ to Ag⁰, and PVP acts as stabilizer protecting the reduced Ag⁰ NPs from further agglomeration. As coupled reaction, H₂O is oxidised to O₂ providing electrons (oxygen evolution reaction, OER) [38,39]. As can be seen from



Fig. 6. Reduction of p-nitrophenol (yellow solution) to p-aminophenol (transparent solution) in the presence of NaBH $_4$ and carbon-supported silver nanoparticles.

Fig. 5, all Ag NPs are well dispersed on the carbon supports with similar particle sizes. Furthermore, there exists the possibility that the size of the Ag NPs would increase during the deposition on the carbon support. Therefore, it can be concluded that these directly synthesized Ag NPs have a particle size of less than 15 nm with an even distribution on the carbon support.

3.2. p-Nitrophenol reduction in the liquid phase

The catalytic activities of the Ag-AC, AC-Ag, Ag-OCNT and OCNT-Ag samples were first examined by the reduction of p-nitrophenol to p-aminophenol in the presence of excess NaBH₄. This reaction is a well-known test reaction and has been widely used to characterize the catalytic activity of functional materials. Metal NPs catalyze this reaction by facilitating electron relay from the donor BH₄ $^-$ to the acceptor p-nitrophenol to overcome the kinetic barrier [40]. As can be seen from Fig. 6, after adding carbon-supported Ag NPs to the solution, the colour of p-nitrophenol changes from yellow to transparent, clearly indicating the reduction from p-nitrophenol to p-aminophenol. The experimental blank tests with pure AC and OCNT samples were also performed. As shown in Fig. S3, it was confirmed that the reduction did not occur in the absence of Ag NPs

Fig. 7 shows typical UV-Vis spectra of the p-nitrophenol reduction with carbon-supported Ag NPs as catalyst. The absorption peak of p-nitrophenol at 400 nm gradually decreased with a concomitant increase of the 300 nm peak of p-aminophenol within 10 min after the addition of carbon-supported Ag NPs to the solution of p-nitrophenol and excess NaBH₄. As can be seen from Fig. 7(a-d) (red line), the 300 nm peak is not present in the absence of supported Ag NPs in the solution.

The amount of NaBH₄ was much higher than that of pnitrophenol during the test. Therefore, the concentration of NaBH₄ is considered to be essentially constant during the whole reaction. The two absorption bands have the two principle components pnitrophenol and p-aminophenol, allowing us to investigate the reaction kinetics by applying pseudo-first order kinetics. The ratio of C_t and C_0 is the ratio of *p*-nitrophenol concentrations at time *t* and 0, which can be derived from the ratio of relative absorption intensity A_t and A_0 . The linear relationship of $ln(C_t/C_0)$ versus time indicates that the reactions follow first-order kinetics. The reaction rate constant is calculated from the slope of each straight line, which varies from 0.2 to 0.4 min⁻¹ (Fig. 7e). The AC-supported Ag NPs show higher reaction rates than the OCNT-supported Ag NPs, which can be explained by the higher Ag loading. There are no significant differences between adding the carbon support before or after the formation of Ag NPs. Overall, all samples achieved high reaction rates demonstrating good catalytic performance.

3.3. Nitrobenzene hydrogenation in the gas phase

In addition to *p*-nitrophenol reduction, the prepared Ag-based catalysts were also employed to catalyse the hydrogenation of nitrobenzene in the gas phase. Nitrobenzene hydrogenation is one of the most widely used approaches to produce aniline with a world-wide production capacity of 5 million metric tons annually, which is mainly used in the manufacture of precursors to polyurethane and other industrial chemicals, such as rubber processing chemicals, herbicides, dyes and pigments [41,42]. The simplified reaction pathway for the hydrogenation of nitrobenzene is shown in Fig. 8. Nitrobenzene is first hydrogenated to nitrosobenzene, subsequently to phenylhydroxylamine and finally to aniline.

The catalytic activities of the catalyst supports, i.e., AC and OCNTs, were first investigated as reference in the hydrogenation of nitrobenzene at temperatures ranging from 250 to 350 °C (see Fig. S4 in Supporting Information). The conversion of nitrobenzene was gradually increased from 0 to 2.2% with increasing the temperature from 250 to 350 °C over AC, and the selectivity was 100% to the partially hydrogenated intermediate nitrosobenzene. The conversion of nitrobenzene (i.e., from 0.4% to 7%) was considerably higher over OCNT than that over AC at all reaction temperatures, which probably can be attributed to the residual growth catalyst in OCNT despite of the intensive washing with nitric acid. The selectivity to aniline was between 60% to 80%, and the other product was nitrosobenzene. The support was stable, and there was only slight deactivation at the highest reaction temperature.

The hydrogenation of nitrobenzene was further investigated with the prepared Ag-based catalysts in the temperature range between of 200 to 350 °C at atmospheric pressure (Fig. 9). The highest conversion of 95% was achieved with OCNT-Ag at 350 °C, whereas only 55% conversion was reached over Ag-AC at the same temperature. The selectivity of aniline was always 100% for both OCNT-based catalysts, while a maximum selectivity of 10% and 20% to nitrosobenzene was observed for AC-Ag and Ag-AC at lower temperatures, respectively. It can be seen that the conversion of nitrobenzene increases with temperature and follows the sequence OCNT-Ag > Ag-OCNT > AC-Ag > Ag-AC in the whole temperature range. In terms of turnover frequency (TOF), the trend for nitrobenzene hydrogenation is even more distinct, that is, OCNT-Ag >> Ag-OCNT >>> AC-Ag > Ag-AC (see Fig. S5 in Supporting Information). In comparison with other Ag-based catalysts (Table S3), the TOF of OCNT-Ag is larger than that of previously reported Ag/TiO2 (i.e., 5.0 vs. 1.2 h^{-1} at 200 °C), but it is lower than that of Ag/Al₂O₃ applied in liquid-phase nitrobenzene hydrogenation, which can be attributed to the much lower nitrobenzene concentration and H₂ pressure (1 bar vs. 30 bar).

Despite the smaller specific surface area and lower Ag loading of OCNT-supported catalysts (Table 1), they showed much better activity for gas-phase nitrobenzene hydrogenation, suggesting superior structural properties. Regarding the catalyst synthesis sequence, it can be concluded that the simultaneous Ag NP formation and deposition on the support is better than the sequential Ag NP formation and deposition: OCNT-Ag > Ag-OCNT and AC-Ag > Ag-AC. Compared with the sequential NPs synthesis-deposition method, the Ag NPs formed by photoreduction were immediately adsorbed on the support during the simultaneous deposition synthesis, which prevented further aggregation of the Ag NPs.

Fig. 9 shows catalyst deactivation in the whole temperature range especially at the highest temperature. All 4 catalysts lose around 30% of their activity during 12 h at 350 °C. It is worthwhile to mention that their deactivation rates are very similar, suggesting the same deactivation mechanism. Sintering of Ag NPs is assumed to be the main reason for the catalyst deactivation. By comparing the Ag particle size before and after reaction (see Fig. 10 for OCNT-Ag and AC-Ag after reaction), it is clear that the Ag particle size

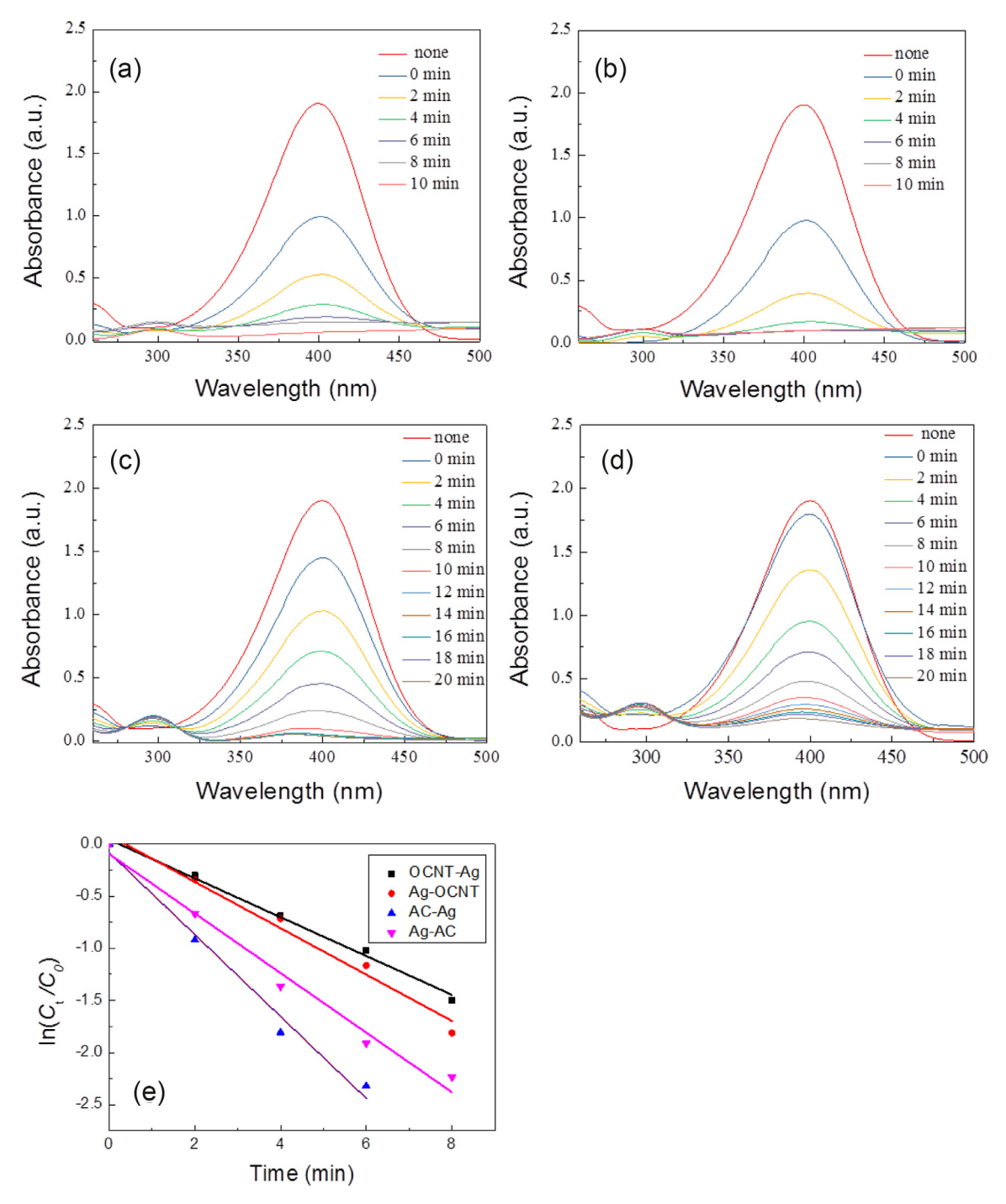


Fig. 7. Time dependent UV absorption spectra for the reduction of p-nitrophenol in the presence of (a) Ag-AC, (b) AC-Ag, (c) Ag-OCNT, (d) OCNT-Ag. (e) Plot of $\ln(C_t/C_0)$ versus time for each sample.

Fig. 8. Simplified reaction pathway for the hydrogenation of nitrobenzene.

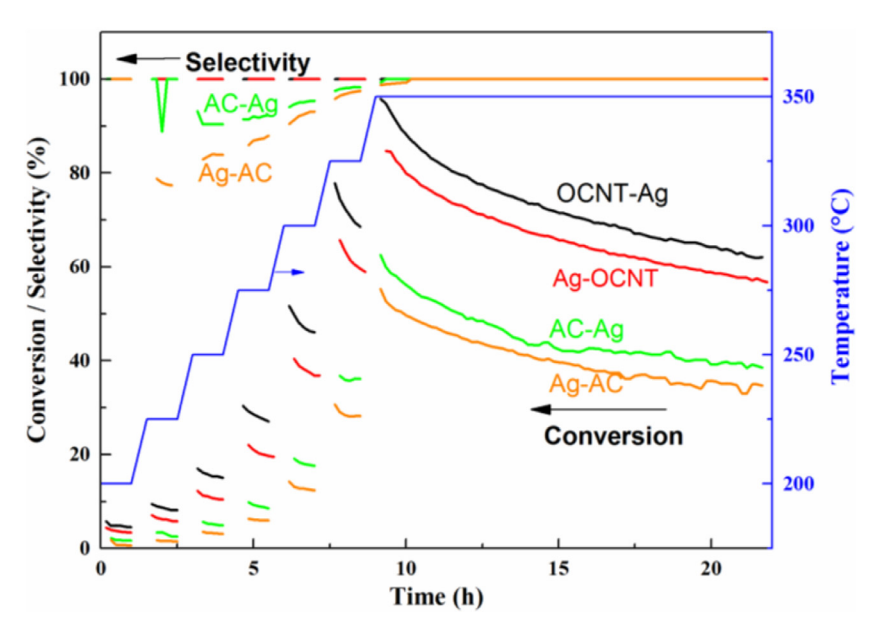


Fig. 9. Conversion and selectivity as a function of reaction time for the hydrogenation of nitrobenzene with Ag-based catalysts. Reaction conditions: 0.1 g catalysts, 0.3 mL/min nitrobenzene, 9 mL/min H₂, temperature from 200 to 350 °C with an interval of 25 °C, 1 h at each temperature except 12 h at 350 °C.

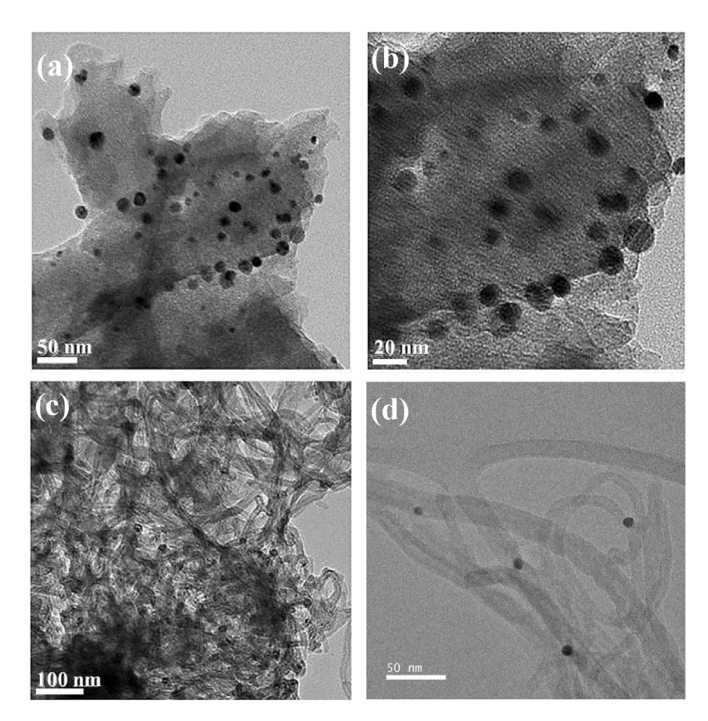


Fig. 10. TEM images of (a, b) AC-Ag and (c, d) OCNT-Ag after nitrobenzene hydrogenation.

increases from 5 to 15 nm to 15–20 nm for OCNT-Ag and AC-Ag. However, other possible deactivation mechanisms like deposition of carbonaceous layers cannot be excluded.

3.4. Oxygen reduction reaction

The development of inexpensive electrocatalysts for the oxygen reduction reaction (ORR) is a key challenge in the conversion of chemical fuels to electricity for many renewable energy con-

version systems such as fuel cells and metal air batteries [43]. Therefore, we studied the electrocatalytic performances of the 4 samples in the ORR (Fig. 11). The linear sweep voltammograms of the Ag-AC, AC-Ag, Ag-OCNT and OCNT-Ag recorded in O2-saturated 0.1 M NaOH solution at a scan rate of 5 mV s⁻¹ under hydrodynamic conditions by means of a rotating disk electrode (RDE) with different rotating speed (100, 400, 900 and 1600 rpm) are shown as Fig. 11(a-d), respectively. The measured current increased with higher rotating speed as expected as a result of faster O2 flux to the electrode surface [44]. The onset potential of the 4 catalysts, defined as the potential corresponding to a current density of $-0.1 \,\mathrm{mA} \,\mathrm{cm}^{-2}$ at the rotating rate of 1600 rpm was in the order AC-Ag (0.908 V) > Ag-OCNT (0.885 V) > OCNT-Ag (0.872 V) >Ag-AC (0.865 V). However, Ag-OCNT required the lowest overpotential (0.700 V) compared with the other samples (OCNT-Ag (0.518 V), Ag-AC (0.478 V) and AC-Ag (0.449 V)) to reach a current density of -3 mA cm⁻². Koutecky-Levich plots of the 4 samples at different potentials (0.2, 0.3, 0.4, 0.5 and 0.6 V) obtained from the corresponding LSVs are presented as the insets of Fig. 11(a-d). All the plots show fairly good linearity, indicating first-order reaction kinetics towards ORR. The number of electrons transferred per O2 molecule in the ORR at the potential of 0.2 V was derived to be 3.55, 3.49, 3.28 and 3.23 for AC-Ag, Ag-OCNT, OCNT-Ag and Ag-AC, respectively. It means that the catalysts favoured the selectivity of the ORR more towards the 4-electron transfer pathway. All prepared 4 samples showed good electrochemical performances, which are very similar to other reported Ag-based materials (Table S4).

4. Conclusions

Ag NPs with typical sizes of 5–15 nm were synthesized by an efficient one-step method without employing reducing agents, which only involves AgNO₃ as precursor, PVP as stabilizer, and AgCl as photocatalyst for providing electrons for Ag⁺ reduction. This synthesis requires only less than 10 min under ambient conditions in aqueous solution, rendering it suitable for continuous process conditions. All parameters are easy to control resulting in the re-

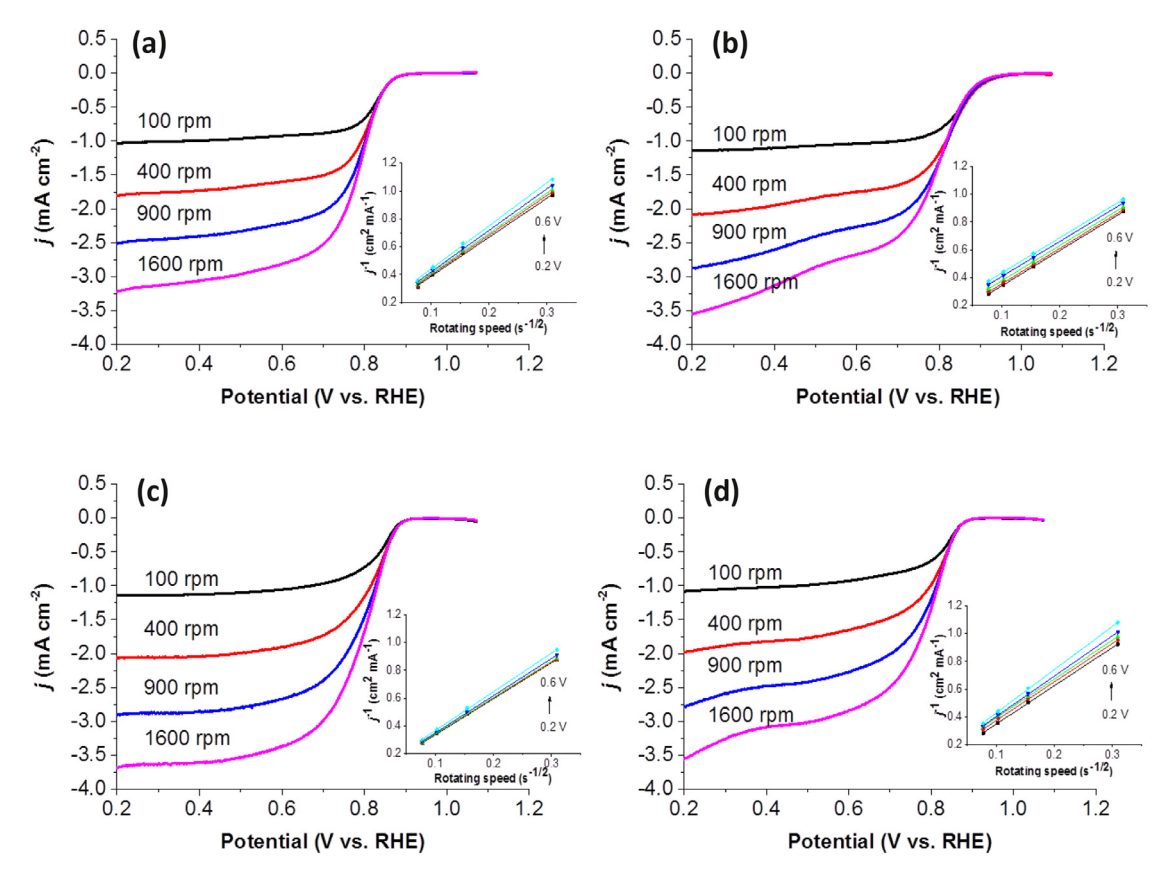


Fig. 11. Linear sweep voltammograms (LSVs, corrected for background currents) recorded in O2-saturated 0.1 M NaOH solution at a scan rate of 5 mV s⁻¹ with different rotating rates (100, 400, 900 and 1600 rpm) showing the electrocatalytic ORR performance of (a) Ag-AC, (b) AC-Ag, (c) Ag-OCNT, and (d) OCNT-Ag.

producible synthesis of Ag NPs with the same physical properties. The Ag NPs were deposited on carbon supports (AC and OCNTs) to form composites as catalyst and applied in the liquid phase in p-nitrophenol reduction, in gas-phase nitrobenzene hydrogenation, and as electrocatalysts in the oxygen reduction reaction. All results demonstrated good catalytic performance. The developed process combines the advantages of photochemical and chemical synthesis, opening a highly efficient way to large-scale synthesis of Ag NPs.

Acknowledgments

The authors appreciate the financial support from the National Natural Science Foundation of China (61574065), Science and Technology Planning Project of Guangdong Province (2016B090906004, 2016B090918083), the Special Fund Project of Science and Technology Application in Guangdong (2017B020240002), graduate student abroad joint training project of South China Normal University. This work has also been partially supported by PCSIRT Project No. IRT_17R40, Guangdong Provincial Key Laboratory of Optical Information Materials and Technology (No. 2017B030301007), MOE International Laboratory for Optical Information Technologies, Shenzhen Science and Technology Plan (No. JSGG20170414143009027), National 111 Project and Guangdong Innovative Research Team Program (No. 2013C102). The authors would like to thank Shuting Xie at South China Normal University for UV-Vis measurement, Dr. Thomas Reinecke and Noushin Arshadi at Ruhr-University Bochum for the XRD and physisorption measurements, respectively.

Supplementary material

Supplementary material associated with this article can be found, in the online version, at doi:10.1016/j.jechem.2019.04.006.

References

- [1] Z.M. Xiu, Q.B. Zhang, H.L. Puppala, V.L. Colvin, P.J.J. Alvarez, Nano. Lett. 12 (2012) 4271–4275.
- [2] X.Z. Liang, P. Wang, M.M. Li, Q.Q. Zhang, Z.Y. Wang, Y. Dai, X.Y. Zhang, Y.Y. Liu, M.H. Whangbo, B.B. Huang, Appl Catal B. 220 (2018) 356-361.
- [3] G.J. Zhao, S.E. Stevens, Biometals 11 (1998) 27-32
- [4] D.S. Choi, A.W. Robertson, J.H. Warner, S.O. Kim, H. Kim, Adv. Mater. 33 (2016) 7115-7122
- [5] P. Yang, J. Zheng, Y. Xu, Q. Zhang, L. Jiang, Adv. Mater. 47 (2016) 10508-10517.
- [6] Y. Su, Y. Xia, Science 5601 (2002) 2176-2179.
- [7] J. Zheng, Y. Ding, B. Tian, Z. Wang, X. Zhuang, J. Am. Chem. Soc. 130 (2008) 10472-10473.
- [8] I. Washio, Y. Xiong, Y. Yin, Y. Xia, Adv. Mater. 13 (2006) 1745-1749.
- [9] Z.S. Pillai, P.V. Kamat, J. Phys. Chem. B 3 (2004) 945-951.
- [10] A. Moshe, G. Markovich, Chem. Mater. 23 (2011) 1239-1245.
- [11] K. Stamplecoskie, J. Scaiano, J. Am. Chem. Soc. 132 (2010) 1825-1827.
- [12] J.A. Creighton, C.G. Blatchford, M.G. Albrecht, J. Chem. Soc., Faraday Trans. 2 1979) 790–798 75.
- [13] D. Kim, S. Jeong, J. Moon, Nanotechnology 17 (2006) 4019-4024.
- [14] S.K. Ghosh, S. Kundu, M. Mandal, S. Nath, T. Pal, J. Nanopart. Res. 5-6 (2003)
- 577-587. [15] L. Huang, M.L. Zhai, D.W. Long, J. Peng, L. Xu, G.Z. Wu, J.Q. Li, G.S. Wei, J. Nanopart, Res. 10 (2008) 1193-1202.
- [16] Y. Zhou, S.H. Yu, C.Y. Wang, X.G. Li, Y.R. Zhu, Z.Y. Chen, Adv. Mater. 10 (1999) 850-852.
- [17] Y. Sun, Y. Yin, B.T. Mayers, T. Herricks, Y. Xia, Chem. Mater. 14 (2002) 4736-4745.
- [18] M. Zhu, C. Wang, D. Meng, G. Diao, J. Mater. Chem. A 1 (2013) 2118–2125.
 [19] J.Q. Hu, Q. Chen, Z.X. Xie, G.B. Han, R.H. Wang, B. Ren, Y. Zhang, Z.L. Yang, Z.Q. Tian, Adv. Funct. Mater. 2 (2004) 183-189.
- [20] A. Panáček, R. Prucek, J. Hrbáč, T. Nevečná, J. Šteffková, R. Zbořil, L. Kvítek, Chem. Mater. 26 (2014) 1332-1339.

- [21] S. Banerjee, K. Loza, W. Meyer-Zaika, O. Prymak, M. Epple, Chem. Mater. 26 (2014) 951-957.
- [22] Z.F. Ren, Z.P. Huang, J.W. Xu, J.H. Wang, P. Bush, M.P. Siegal, P.N. Provencio, Science 5391 (1998) 1105–1107.
- [23] K. Gong, F. Du, Z. Xia, M. Durstock, L. Dai, Science 5915 (2009) 760-764.
- [24] N. Li, X. Chen, L. Stoica, W. Xia, J. Qian, J. Assmann, W. Schuhmann, M. Muhler, Adv. Mater. 19 (2007) 2957–2960.
- [25] P. Chen, T. Xiao, Y. Qian, S. Li, S. Yu, Adv. Mater. 23 (2013) 3192-3196.
- [26] K. Woan, G. Pyrgiotakis, W. Sigmund, Adv. Mater. 21 (2009) 2233–2239.
- [27] Z. Wen, J. Liu, J. Li, Adv. Mater. 4 (2008) 743–747.
- [27] Z. Weil, J. Lid, J. Li, J. Vang, Y. Zhang, H. Li, Electrochem. Commun. 6 (2008) 876–879.
 [29] N. Li, Q. Xu, M. Zhou, W. Xia, X. Chen, M. Bron, W. Schuhmann, M. Muhler, Electrochem. Commun. 7 (2010) 939–943.
- [30] E.S. Steigerwalt, G.A. Deluga, D.E. Cliffel, C.M. Lukehart, J. Phys. Chem. B 105 (2001) 8097-8101.
- [31] J. Liu, S. Fu, B. Yuan, Y. Li, Z. Deng, J. Am. Chem. Soc. 21 (2010) 7279–7281.
- [32] C. Pacholski, A. Kornowski, H. Weller, Angew. Chem. Int. Ed. 36 (2004) 4774-4777
- [33] W. Xia, C. Jin, S. Kundu, M. Muhler, Carbon 47 (2009) 919-922.

- [34] C. An, S. Peng, Y. Sun, Avd. Mater. 23 (2010) 2570-2574.
- [35] T. Tadaaki, J. Soc, Photogr. Sci. Technol. Jpn. 72 (2009) 88-94.
- [36] D. Schuerch, A. Currao, Chimia 57 (2003) 204–207.
- [37] B. Cai, J. Wang, S. Gan, D. Han, Z. Wu, L. Niu, J. Mater. Chem. A 2 (2014) 5280-5286.
- [38] V. Kumar, T. Uchida, T. Mizuki, Y. Nakajima, Y. Katsube, T. Hanajiri, T. Maekawa, Adv. Nat. Sci.: Nanosci. Nanotechnol. 7 (2016) 015002–015014.
- [39] V.R. Reddy, A. Currao, G. Calzaferri, in: Journal Physics Conference Series, 61, 2007, pp. 960-965.

- 2007, pp. 900–903.
 40] Z.K. Zheng, T. Tachikawa, T. Majima, J. Am. Chem. Soc 137 (2015) 948–957.
 [41] S.W.T. Price, K. Geraki, K. Ignatyev, P.T. Witte, A.M. Beale, J.F.W. Mosselmans, Angew. Chem. Int. Ed. 54 (2015) 9886–9889.
 [42] P. Chen, A. Khetan, F. Yang, V. Migunov, P. Weide, S.P. Stuermer, P. Guo, K. Kaehler, W. Xia, J. Mayer, H. Pitsch, U. Simon, M. Muhler, ACS Catal. 7 (2017) 1107–1206. 1197-1206.
- [43] I. Katsounaros, S. Cherevko, A.R. Zeradjanin, K.J.J. Mayrhofer, Angew. Chem. Int. Ed. 26 (2014) 102-121.
- [44] B.C. He, X.X. Chen, J.M. Lu, S.D. Yao, J. Wei, Q. Zhao, D.S. Jing, X.N. Huang, T. Wang, Electroanalysis 28 (2016) 2435–2443.